

## **Supplementary material: Nanoscale imaging of the full strain tensor of specific dislocations extracted from a bulk sample**

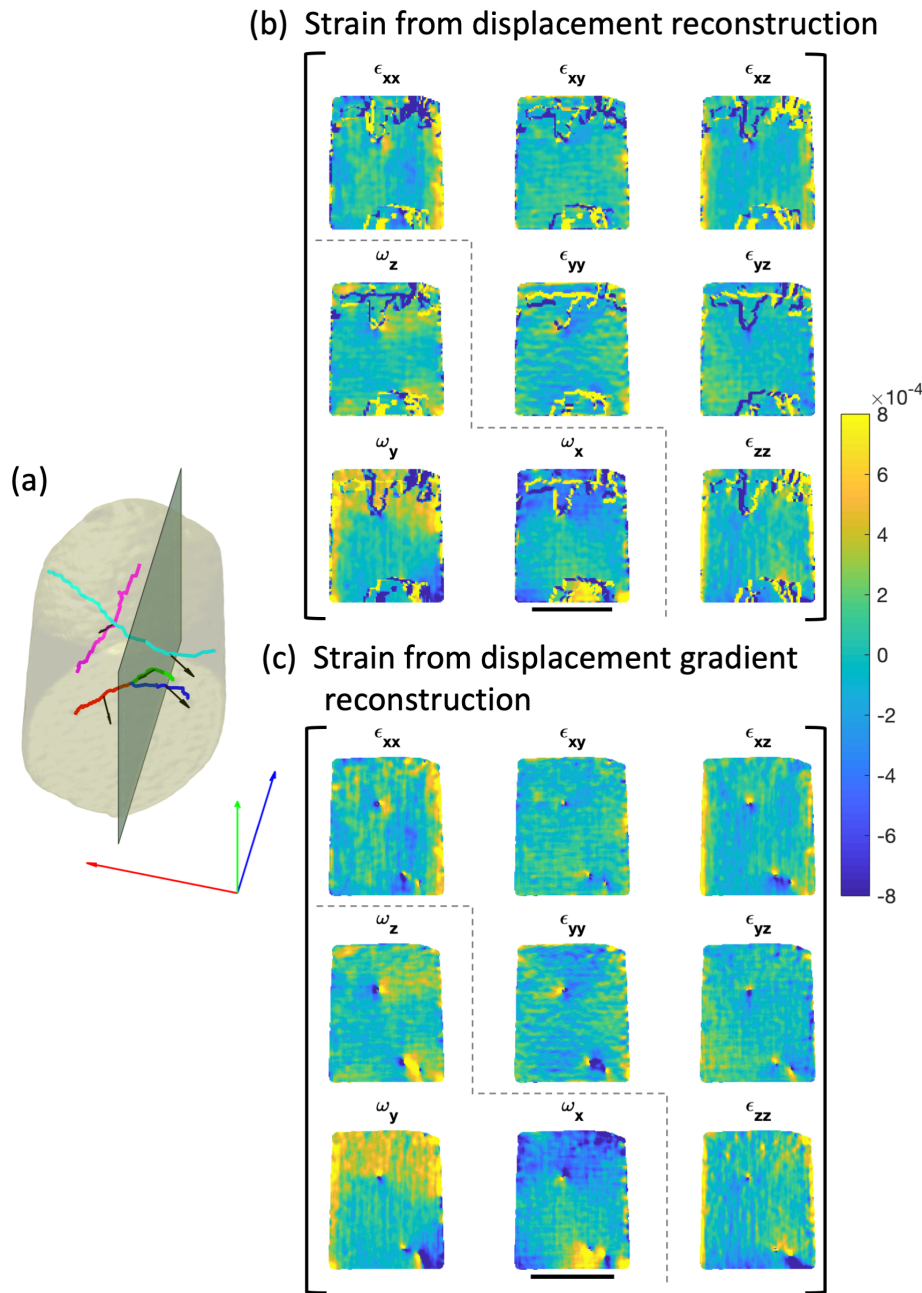
Felix Hofmann<sup>1</sup>, Nicholas W. Phillips<sup>1</sup>, Suchandrima Das<sup>1</sup>, Phani Karamched<sup>2</sup>, Gareth M. Hughes<sup>2</sup>, James O. Douglas<sup>2</sup>, Wonsuk Cha<sup>3</sup>, Wenjun Liu<sup>3</sup>

<sup>1</sup> Department of Engineering Science, University of Oxford, Parks Road, Oxford, OX1 3PJ, UK

<sup>2</sup> Department of Materials, University of Oxford, Parks Road, Oxford, OX1 3PH, UK

<sup>3</sup> Advance Photon Source, Argonne National Lab, 9700 S. Cass Avenue, Lemont, Illinois 60439, USA

**Supplementary figure:**



**Supplementary Figure S1:** 3D strain fields computed using different approaches. (a) 3D rendering of the sample and dislocations contained within it. The red, green and blue arrows point in the x, y and z directions respectively and are plotted with a length of 500 nm. Superimposed is the y-z section through the crystal on which strains in (b) and (c) are plotted. (b) Lattice strains and lattice rotations calculated by differentiation of the displacement field reconstructed from multi-reflection BCDI measurements. (c) Lattice strains and rotations computed based on the 3D-resolved displacement gradient reconstruction approach described in this paper. Comparison of (b) and (c) highlights large spurious strains and rotations in (b) due to discontinuities in the lattice displacement associated with dislocations. The same colour scale applies to (b) and (c), with lattice rotations plotted in radians. Scalebars in (b) and (c) are 500 nm in length.

**Supplementary movie captions:**

**Supplementary movie SM1:** Diffraction data from the  $(110)$  reflection after alignment and summing of repeated scans, and correction for detector deadtime and pixel sensitivity. Intensity is shown on a log-scale.

**Supplementary movie SM2:** Diffraction data from the  $(1\bar{1}0)$  reflection after alignment and summing of repeated scans, and correction for detector deadtime and pixel sensitivity. Intensity is shown on a log-scale.

**Supplementary movie SM3:** Diffraction data from the  $(\bar{1}0\bar{1})$  reflection after alignment and summing of repeated scans, and correction for detector deadtime and pixel sensitivity. Intensity is shown on a log-scale.

**Supplementary movie SM4:** Diffraction data from the  $(10\bar{1})$  reflection after alignment and summing of repeated scans, and correction for detector deadtime and pixel sensitivity. Intensity is shown on a log-scale.

**Supplementary movie SM5:** Diffraction data from the  $(0\bar{1}\bar{1})$  reflection after alignment and summing of repeated scans, and correction for detector deadtime and pixel sensitivity. Intensity is shown on a log-scale.

**Supplementary movie SM6:** Diffraction data from the  $(01\bar{1})$  reflection after alignment and summing of repeated scans, and correction for detector deadtime and pixel sensitivity. Intensity is shown on a log-scale.

**Supplementary movie SM7:** Recovered 3D crystal morphology. Semi-transparent 3D rendering of the electron density amplitude recovered from BCDI measurements of six different reflections. Dislocations can be readily identified as pipes of missing intensity in different reflections. The scattering vector direction is superimposed for each reflection (black arrow). Red, green and blue arrows indicate the directions of the x, y, z axes respectively and are plotted with a length of 500 nm.

**Supplementary movie SM8:** 3D dislocation structures. Semi-transparent rendering of the average electron density amplitude recovered from BCDI measurements of six different reflections. Superimposed are the five dislocation lines that were segmented: 1 (magenta), 2 (cyan), 3 (red), 4 (green) and 5 (blue). For each dislocation a black arrow indicating the direction of Burgers vector is superimposed. Red, green and blue arrows indicate the directions of the x, y, z axes respectively and are plotted with a length of 500 nm.

**Supplementary movie SM9:** Reconstructed lattice strains and rotations. Virtual slices in the z-y plane (horizontal axis – vertical axis) through the crystal plotted as a function of x position. On each slice the six components of the full lattice strain tensor are shown (upper triangle and diagonal). Also plotted are the three components of the lattice rotation tensor (lower triangle). Lattice distortions associated with dislocations are clearly visible. Within ~25 nm of the surface spurious strains due to FIB machining can be identified. The colour bar applies to all plots with lattice rotations shown in radians. The axis scale is in nm.

**Supplementary movie SM10:** Virtual y-z section through the crystal. Semi-transparent rendering of the average electron density amplitude recovered from BCDI measurements of six different reflections. Superimposed are the five dislocation lines that were segmented, using the same colour coding as in Fig. 3(b). For each dislocation a black arrow indicating the direction of Burgers vector is superimposed. Also shown is a semi-transparent green plane, indicating the position of the virtual slice through the crystal on which strains in Fig. 5(b) and (c) are plotted. Red, green and blue arrows indicate the directions of the x, y, z axes respectively and are plotted with a length of 500 nm.

**Supplementary movie SM11:** Predicted lattice strains and rotations. Virtual slices through the crystal in the z-y plane (horizontal axis – vertical axis) plotted as a function of x position. Shown on each slice are the six components of the lattice strain tensor (upper triangle and diagonal) predicted by a linear elastic model of the 3D dislocation structure. The three components of the lattice rotation tensor predicted by this model are also shown (lower triangle). The positioning of slices, colour scale and length-scale are the same as for the experimentally measured lattice distortions shown in supplementary movie SM3. Horizontal and vertical axes show length in nm.